Supplementary material

Almost-solid-state electrolyte with quadruple-hydrogen-bond-based semi-interpenetrating network for lithium metal batteries

Zhongxiu Li [1], Yong Wang [1], Yu Li [2]* and Wei Feng [1]*

1.School of Materials Science and Engineering, Tianjin University, Tianjin 300072, China

2.Institute of Advanced Technology and Equipment, Beijing University of Chemical Technology, Beijing 100029, China

·Corresponding authors

Emails: 2022500016@buct.edu.cn (Y. Li); weifeng@tju.edu.cn (W. Feng)

1. EXPERIMENTAL SECTION

1.1 Materials

2-Amino-6-methyl-4-pyrimidinol (AMP, 99%, Heowns Tianjin Co., Ltd.), PEG (M_n ~ 4000, Aladdin Holdings Group Co., Ltd.) and Dibutyltin dilaurate (DBTDL, ≥ 98%, Aladdin Holdings Group Co., Ltd.) were stored in a chemical reagent desiccator. Petroleum ether (AR), Acetone (AR), and Ethanol (≥ 99.5%, anhydrous grade, H_2O < 0.005%) were purchased from Tianjin Jiangtian Chemical Technology Co., Ltd. Hexamethylene diisocyanate (HDI, 99%), N-N-Dimethylacetamide (DMAc, 99.8%), 2,2'-Azobis(2-methylpropionitrile) (AIBN, 98%), PEGMA (M_n ~ 950) and CEA (95%) were purchased from Shanghai Macklin Co., Ltd. LiTFSI (Kolud Technology Co., Ltd.), N-methylpyrrolidone (NMP, Adams), conductive carbon black Super P (Guangdong Canrd New Energy Technology Co., Ltd. Dimethyl), 1.0 M LiTFSI in ethylene carbonate (EC): diethylcarbonate (DEC) = 1:1 vol % (ρ = 1.2897 ± 0.01g cm^{-3}, Canrd New Energy Technology Co., Ltd.), lithium metal (99.9%, diameter (d) = 15.6 ± 0.3 mm, thickness (L) = 0.50 ± 0.02 mm, China Energy Lithium Co., Ltd.), LFP (98%, Macklin Co., Ltd.) and poly(1,1-difluoroethylene) (PVDF-HSV900, Arkema) were stored in a glove box.

1.2 Synthetic process

1.2.1 Preparation of macromolecular plasticizers.

According to Fig. S1, with a molar ratio of AMP to HDI of 1:6, the reaction was carried out under a continuous flow of argon at 100°C with stirring for 24 hours. Following the reaction, the resulting white powder was purified by washing with petroleum ether and acetone three times and filtering to remove unreacted monomers, yielding a white needle-like solid powder identified as UPyNCO.

Then, following a molar ratio of 2.2:1, the UPyNCO obtained from the first step and PEG were each dissolved in DMAc. After stirring until a clear and transparent solution was achieved, 2 ~ 3 drops of DBTDL were added as a reaction catalyst. The mixture was then reacted at 70℃ for 10 hours. The product was rotary evaporated at 80℃ to remove most of the unreacted small molecules, yielding a white solid which is the end-capped product UPU.

With a molar ratio of AMP to HDI of 2.2:1, under a continuous flow of argon, HDI was added dropwise to the reaction mixture at 100℃ with constant stirring. After 24 hours of reaction, the resulting white product was washed three times with petroleum ether and acetone,

followed by filtration to remove any unreacted monomers. The white solid obtained was URU, see Fig. S7–S8.

1.2.2 Preparation of SPEs

Using AIBN as the initiator and DMAc as the solvent, the monomers PEGMA, PEGMA\CEA, PEGMA\CEA\URU, and PEGMA\CEA\UPU were each dissolved in solutions. In each mixture, AIBN accounts for 0.5 wt% of the total mass of the monomers, and the molar ratio of the copolymer monomers PEGMA to CEA was 1:2. Regardless of the system, the molar ratio of EO_{PEG} to Li^+ was designed to be 15:1. The thermal polymerization of PEGMA and CEA is shown in Fig. 1b. Also, URU and UPU were individually and uniformly dispersed in the monomer solution before polymerization. After thorough stirring at room temperature (RT) for 6 hours to obtain a homogeneous solution, the reactions were carried out at 70℃ for 10 hours. The mixtures were then transferred into Teflon culture dishes, vacuum dried at 60°C for 10 hours, and further vacuum dried at 70°C for 24 hours. Finally, the PPEGMA, P(PEGMA-CEA), P(PEGMA-CEA)@URU, and P(PEGMA-CEA)@UPU SPEs membranes were peeled off from the Teflon substrate for characterization and used for the subsequent assembly of CR2032-type batteries.

1.2.3 Preparation of the cathodes

For the preparation of LFP cathodes, a mixture of LFP, Super P, and PVDF in a weight ratio of 8:1:1 was subjected to intensive milling to ensure a uniform blend. Subsequently, an adequate volume of NMP was introduced to achieve a consistent slurry, which was then uniformly spread onto aluminum foil using a doctor blade. The coated foil was subsequently introduced into a vacuum oven set at a temperature of 120℃ for a duration of 24 hours to facilitate the drying process under vacuum conditions. Upon completion of the drying phase, the resultant LFP cathode material was trimmed into circular segments, each with an active material loading of 1.5–3.0 mg cm^{-2}.

1.2.4 The assembly process of CR2032 batteries

In a CR2032 battery, SPE was placed between the lithium metals, as well as between the lithium metal and the LFP cathode, to assemble symmetric lithium batteries and LFP batteries respectively. Liquid electrolyte (1.0 M LiTFSI in EC : DEC = 1:1 vol%, ρ = 1.2897 ± 0.01g cm^{-3}) was applied between the electrolyte and electrode, with a total volume of 0.5 μL (Table S1 and Note S1). The

assembled battery was then heated on a hot plate at 60°C for 12 hours to ensure thorough impregnation of the electrolyte into the electrode interfaces. Subsequently, the battery was left to stand at room temperature for 24 h before undergoing cycling and rate capability testing.

Table S1 Parameters of the various components used in assembling the battery.

SPEs	PPEGMA	P(PEGMA-CEA)	P(PEGMA-CEA)@URU	P(PEGMA-CEA)@UPU
Average mass of SPE (m_{SPE}) [g]	0.0248	0.0287	0.0325	0.0344
Mass of the added LE (m_{LE}) [g]	0.0006	0.0006	0.0006	0.0006
The content of LE [wt%]	2.36	2.05	1.81	1.71

Note S1: The calculation method for liquid content：

$$The\ content\ of\ LE\ =\ \frac{m_{LE}}{m_{SPE}\ +\ m_{LE}} \qquad (1)$$

1.3 Characterization

1.3.1 Material characterization

The molecular structures of UPyNCO, UPU, PEGMA, CEA, and P(PEGMA-CEA) were elucidated using ^{1}H NMR on a BRUKER AVANCE III HD 500 instrument, with deuterated chloroform ($CDCl_3$) serving as the solvent. FTIR spectroscopy was performed using a Bruker Tensor II; sample preparations were conducted via the potassium bromide (KBr) pellet method, with a measurement range spanning from 4000 to 400 cm^{-1}. TG analysis (TGA) was performed under an nitrogen atmosphere at a heating rate of 10℃ min^{-1} from 30 to 600 ℃ using Netzsch STA449F3. The surface morphology of SPEs as well as that of the Li metal after cycling were examined using SEM (Regulus 8100, Hitachi, Japan). The phase composition of the PEs was characterized by XRD (Rigaku SmartLab SE, Japan) over a 2θ range of 10 to 80°. The lithium metal was soaked in a blank electrolyte within an argon-filled glove box to remove residual electrolyte and lithium salts. The chemical states of carbon, oxygen, fluorine, and nitrogen in the SEI layer on the surface of the cycled lithium metal were analyzed using XPS (Thermo Scientific K-Alpha +, USA). Tensile tests of the SPEs were tested using a universal testing machine (UTM2203, Shenzhen Suns Technology Stock Co., Ltd.). DSC was conducted on a NETZSCH DSC 200F3 system from –60 to 120℃. The molecular weights of the polymer and its distribution were determined by GPC using Agilent 1290 Infinity II GPC.

1.3.2 Electrochemical measurement

The ionic conductivity (σ) of SPEs was measured by EIS using Zahner Zennium Pro electrochemical workstation. SPE was placed between stainless steel (SS) assembled into in SS|SPE|SS battery and tested from 25 to 80°C at frequencies of 10k ~ 8M Hz with a 10 mV perturbation. The σ was calculated using Equation (2):

$$\sigma = L/R_b S \tag{2}$$

where L represents the thickness of the SPE, S denotes the area of the SPEs, and R_b indicates the intrinsic resistance of the electrolyte.

The relationship between ionic conductivity and temperature was analyzed using the following VTF equation:

$$\sigma = \sigma_0 T^{-1/2} \cdot \exp\left[\frac{-B}{k_B(T - T_0)}\right] \tag{3}$$

where σ_0 is the pre-exponential factor related to the number of charge carriers, B is the constant related to the activation energy of the chain segment and T_0 is the glassy phase transition temperature in thermodynamic equilibrium, which is usually 30 – 50 K lower than the actual measured value.

The Li^+ transference number (t_{Li+}) of the electrolyte was measured by EIS and DC polarization. The Li|SPE|Li battery was tested at a polarization voltage of 10 mV for 2 h at 25°C. The final t_{Li+} was calculated using Equation (4):

$$t_{Li^+} = \frac{I_s(\Delta V - I_0 R_0)}{I_0(\Delta V - I_s R_s)} \tag{4}$$

where I_o and I_s represent the initial and steady-state currents, respectively. R_o and R_s are the impedances, before and after polarization, respectively. ΔV denotes the voltage applied across the battery.

The ESW of SPEs (PEGMA, P(PEGMA-CEA), P(PEGMA-CEA)@URU and P(PEGMA-CEA)@UPU) were evaluated using LSV. Specifically, the electrolyte was set up between lithium and SS to create a Li|SPE|SS battery configuration, which was then examined using LSV at ambient temperature over a potential sweep of 0–7 V at a scanning speed of 1 mV s^{-1}.

The CCD test was conducted on a LANDT CT2001A battery testing system based

on a constant charge/discharge capacity of 0.1 mAh cm^{-2}, with the current gradually increased from 0.05 mA cm^{-2} to 1 mA cm^{-2} in steps of 0.025 mA cm^{-2}, 0.05 mA cm^{-2}, and 0.1 mA cm^{-2}.

The charge/discharge tests of the LFP batteries were performed on a LANDT CT2001A battery testing system between 2.5–4.0 V at 25°C.

1.3.3 Density Functional Theory calculations

DFT calculations were performed using the ORCA 5.0.4 software package. [1] The B3LYP-D3(BJ)/def2-SVP basis set was employed to initially optimize the structure. Subsequently, the optimized structure was used to carry out single-point energy calculations with the B3LYP-D3(BJ)/def2-TZVPPD basis set. After the calculations were completed, the HOMO and LUMO energy levels of the molecules were extracted. [2-4] Visualization of the structures was obtained using Avogadro 1.2.0 software. [5]

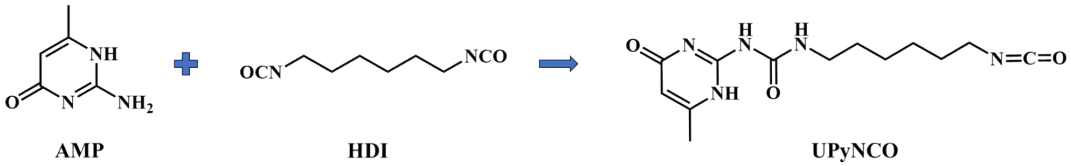

Fig. S1 Schematic diagram of the preparation of UPyNCO.

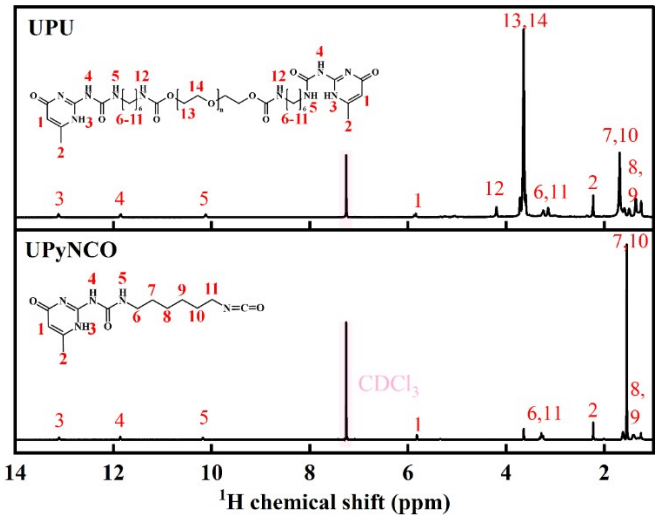

Fig. S2 ^{1}H NMR spectra of the main components in the UPyNCO and UPU.

(The H chemical shift of $CDCl_3$ is 7.26 ppm)

Fig. S3 Difference in the appearances of the liquid precursor solution before and after the polymerization.

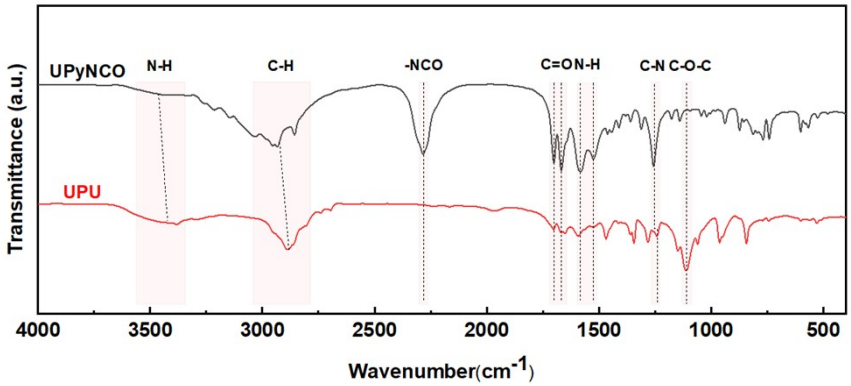

Fig. S4 FTIR spectra of the main components in the UPyNCO and UPU.

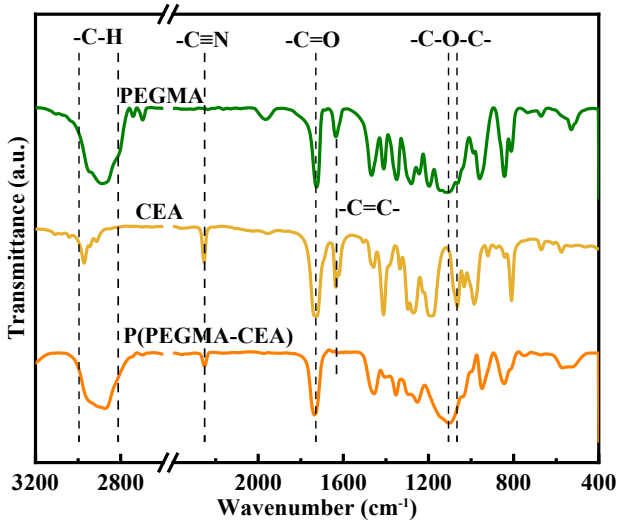

Fig. S5 FTIR spectra of the main components in the PEGMA monomer, CEA monomer and P(PEGMA-CEA) copolymer.

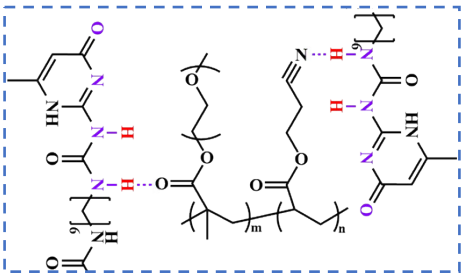

Fig. S6 Schematic illustration of hydrogen bonding between UPy unit and P(PEGMA-CEA) copolymer.

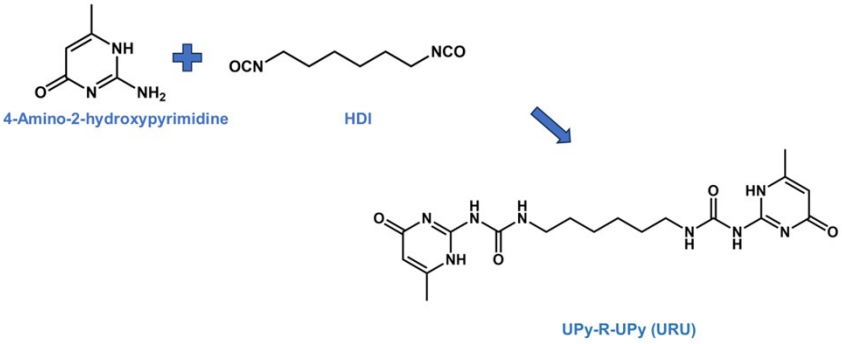

Fig. S7 Schematic diagram of the preparation of URU.

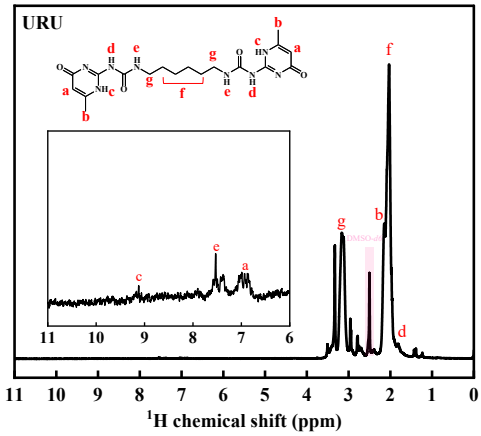

Fig. S8 ^{1}H NMR spectra of the main components in the URU.

(The H chemical shift of DMSO-d6 is 2.50 ppm)

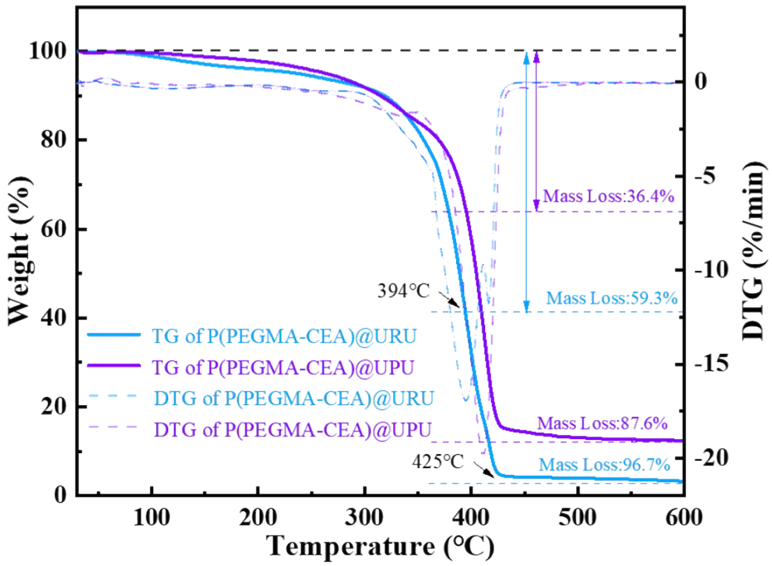

Fig. S9 TG and DTG curves of P(PEGMA-CEA)@URU and P(PEGMA-CEA)@UPU

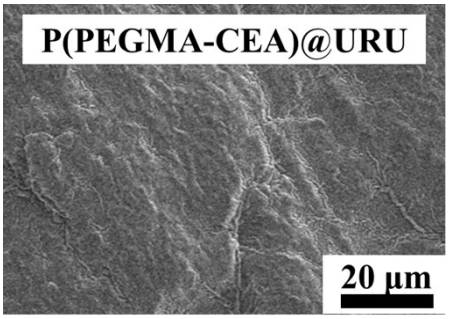

Fig. S10 The SEM images of surface morphology for P(PEGMA-CEA)@URU SPE.

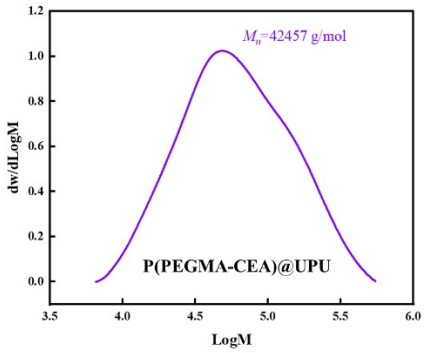

Fig. S11 GPC spectra of P(PEGMA-CEA)@UPU SPE.

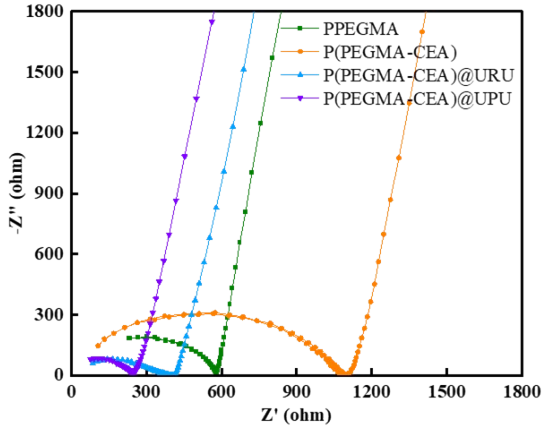

Fig. S12 EIS plot of SPEs at room temperature.

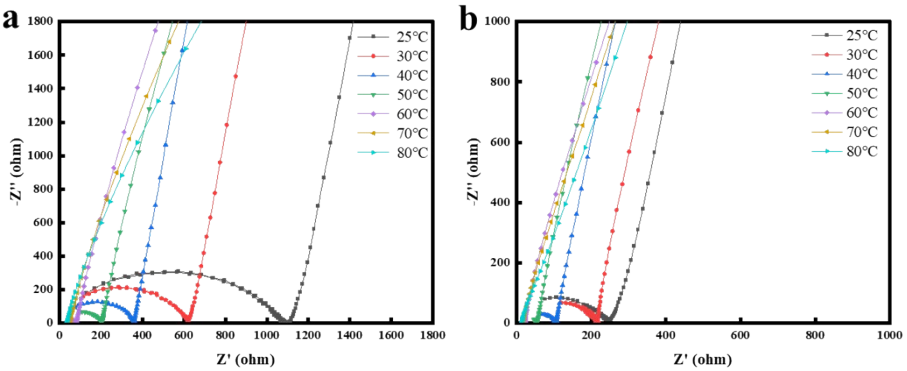

Fig. S13 EIS plot of P(PEGMA-CEA) and P(PEGMA-CEA)@UPU SPEs at different temperatures.

Fig. S14 Thickness of SPE membranes.

Table S2 Thickness (L), diameter (d), intrinsic resistance (R_b) and ionic conductivity (σ) of SPEs at room temperature.

Temperature (°C)	L (mm)	d (mm)	R_b (Ω)	σ (S·cm^{-1})
PPEGMA	0.173	16	583.1	1.48 × 10^{-5}
P(PEGMA-CEA)	0.329	16	1093.2	1.51 × 10^{-5}
P(PEGMA-CEA)@URU	0.339	16	405.2	4.19 × 10^{-5}
P(PEGMA-CEA)@UPU	0.304	16	244.8	6.21 × 10^{-5}

Table S3 Thickness (L), diameter (d), intrinsic resistance (R_b) and ionic conductivity (σ) of P(PEGMA-CEA) SPE at different temperatures.

Temperature (°C)	L (mm)	d (mm)	R_b (Ω)	σ (S·cm^{-1})
25°C	0.329	16	1092.9	1.51 × 10^{-5}
30°C	0.329	16	613.8	2.68 × 10^{-5}
40°C	0.329	16	351.6	4.68 × 10^{-5}
50°C	0.329	16	203.1	8.10 × 10^{-5}
60°C	0.329	16	77.96	2.11 × 10^{-4}
70°C	0.329	16	47.1	3.50 × 10^{-4}
80°C	0.329	16	33.98	4.84 × 10^{-4}

Table S4 Thickness (L), diameter (d), intrinsic resistance (R_b) and ionic conductivity (σ) of P(PEGMA-CEA)@UPU SPE at different temperatures.

Temperature (°C)	L (mm)	d (mm)	R_b (Ω)	σ (S·cm^{-1})
25°C	0.304	16	244.8	6.21 × 10^{-5}
30°C	0.304	16	210.8	7.21 × 10^{-5}
40°C	0.304	16	105.9	1.44 × 10^{-4}
50°C	0.304	16	50.2	3.03 × 10^{-4}
60°C	0.304	16	23.0	6.61 × 10^{-4}
70°C	0.304	16	18.0	8.44 × 10^{-4}
80°C	0.304	16	16.0	9.50 × 10^{-4}

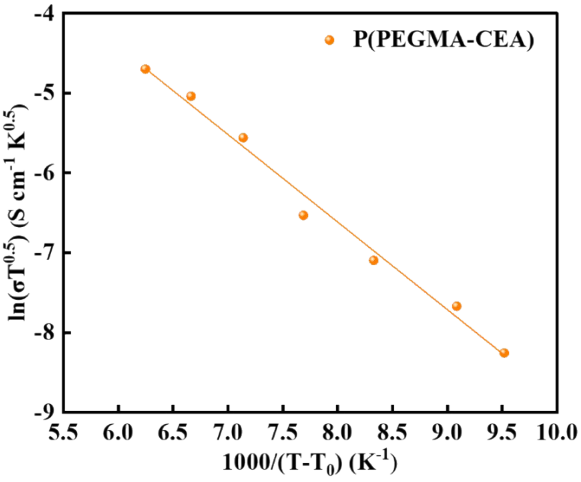

Fig. S15 VTF equation fitting curve of P(PEGMA-CEA) at 25–80°C.

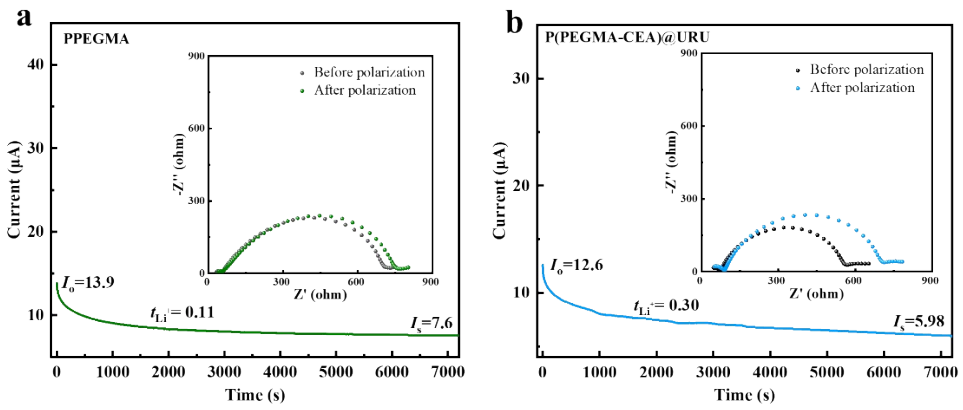

Fig. S16 The I-t curves obtained from Li|PPEGMA |Li and Li|P(PEGMA-CEA)@URU|Li symmetric battery tested at 0.010 V polarization voltage, and the inset corresponds to the Nyquist plots of the SPEs before and after polarization.

Table S5 I_o, I_s, R_o and R_s of the Li|SPE|Li battery at 25℃.

Electrolyte	I_o (μA)	I_s (μA)	R_o (Ω)	R_s (Ω)	t_{Li+}
PPEGMA	13.9	7.6	648	697	0.11
P(PEGMA-CEA)	16.5	8.2	421	444	0.24
P(PEGMA-CEA)@URU	12.6	5.98	489	670	0.30
P(PEGMA-CEA)@UPU	23.7	17.4	331	430	0.63

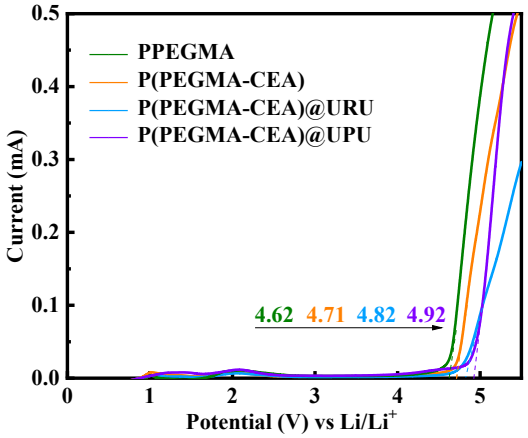

Fig. S17 LSV curves of PPEGMA, P(PEGMA-CEA), P(PEGMA-CEA)@URU and P(PEGMA-CEA)@UPU SPEs.

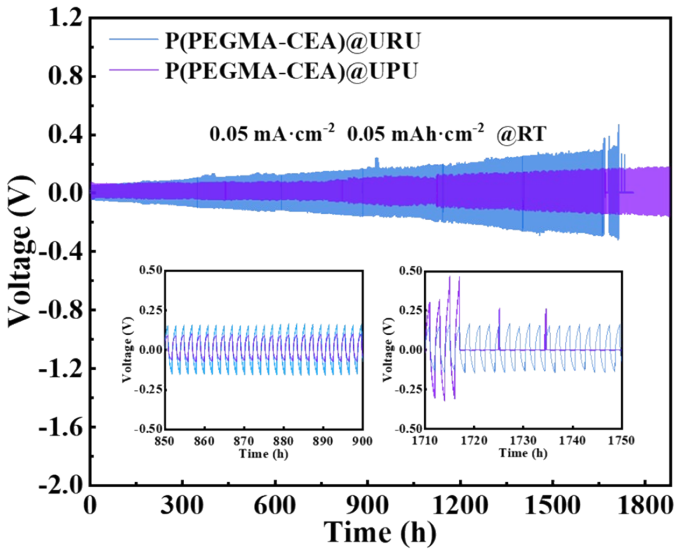

Fig. S18 Voltage profiles of the Li|P(PEGMA-CEA)@URU|Li and Li|P(PEGMA-CEA)@UPU|Li batteries during lithium plating/striping at current densities of 0.05 mA cm^{-2} at room temperature; insets–Different times of the selected voltage profiles.

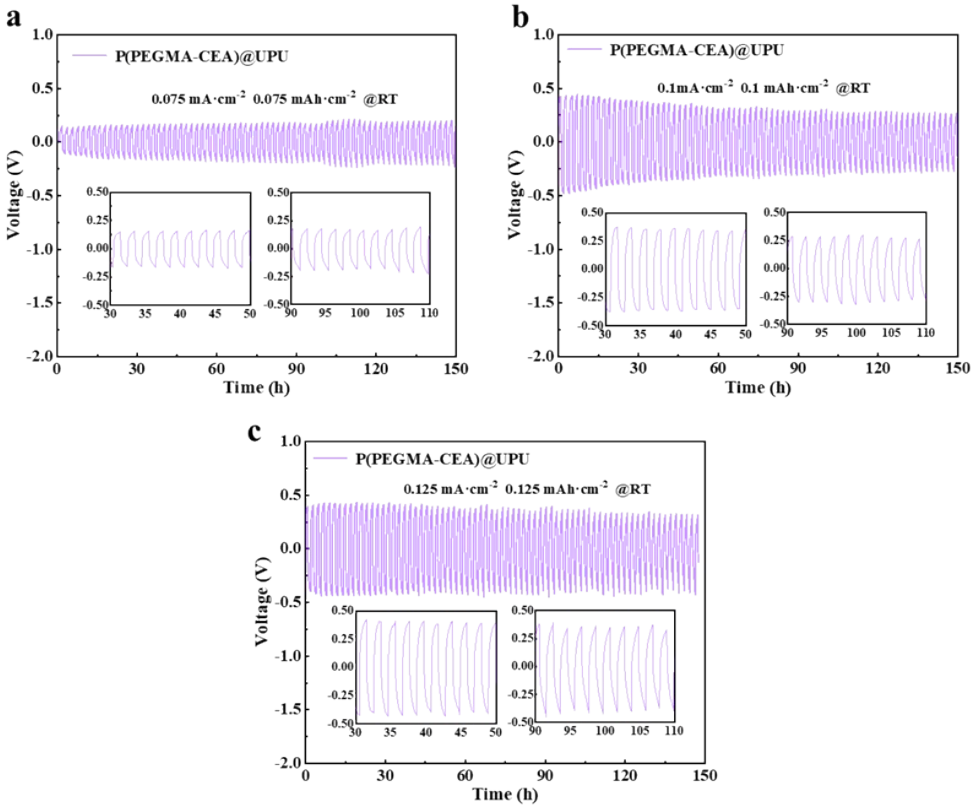

Fig. S19 Voltage profiles of the Li|P(PEGMA-CEA)@UPU|Li battery during lithium plating/striping at current densities of 0.075, 0.1 and 0.125 mA cm^{-2} at room temperature; insets–Different times of the selected voltage profiles.

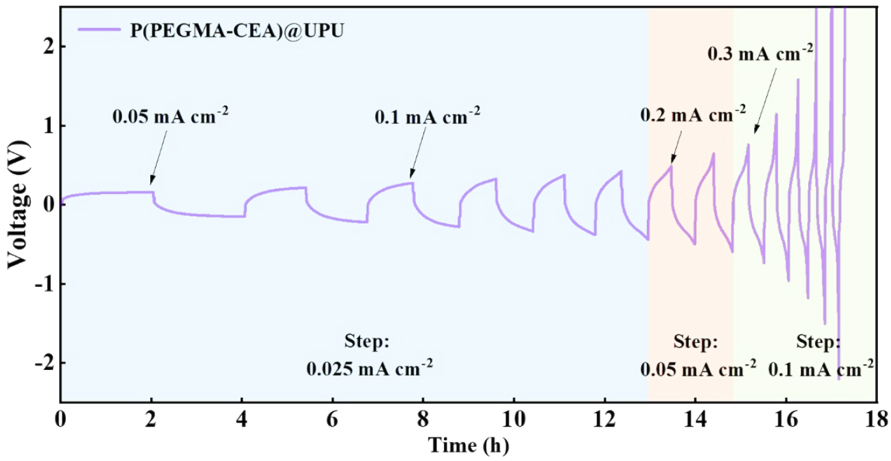

Fig. S20 CCD test of the Li|P(PEGMA-CEA)@UPU|Li battery.

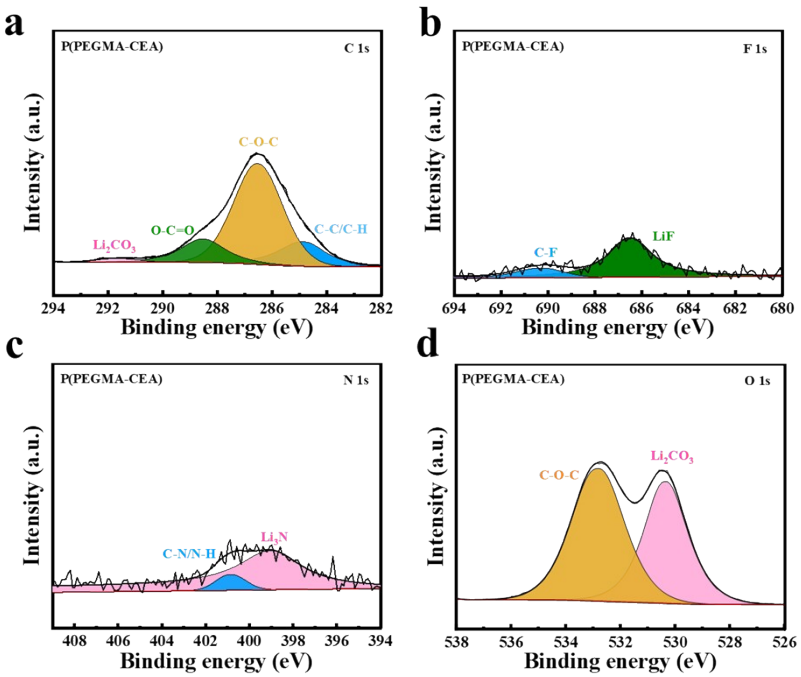

Fig. S21 The XPS spectra of (a) C 1s, (b) F 1s, (c) N 1s and (d) O 1s spectra of the SEI recorded after the cycling of the Li|P(PEGMA-CEA)|Li battery.

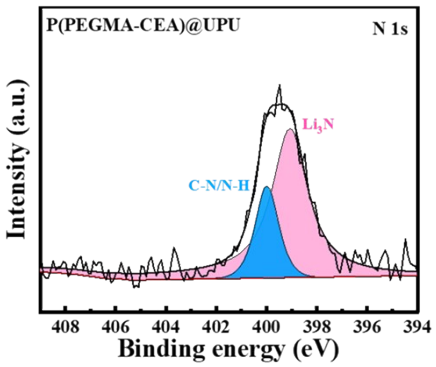

Fig. S22 The XPS spectra of N 1s in SEI after cycling of Li|P(PEGMA-CEA)@UPU|Li symmetric battery.

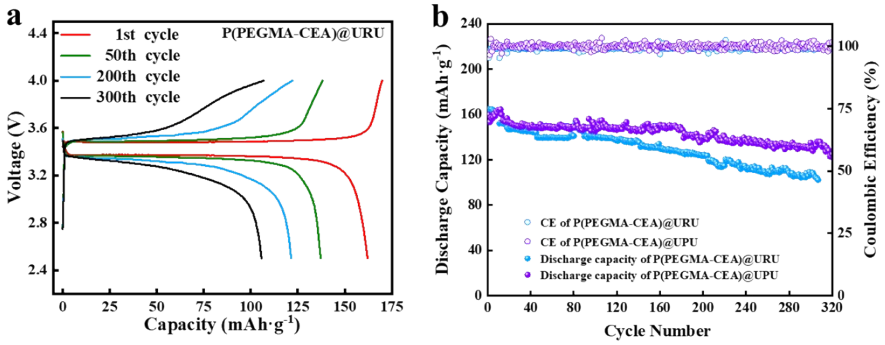

Fig. S23 (a) Typical charge/discharge curves of the Li|P(PEGMA-CEA)@URU|LFP battery at 2.5–4.0 V. (b) Cycling performance and coulombic efficiency of the Li|P(PEGMA-CEA)@URU|LFP and Li|P(PEGMA-CEA)@UPU|LFP batteries at 25 °C and 0.2 C.

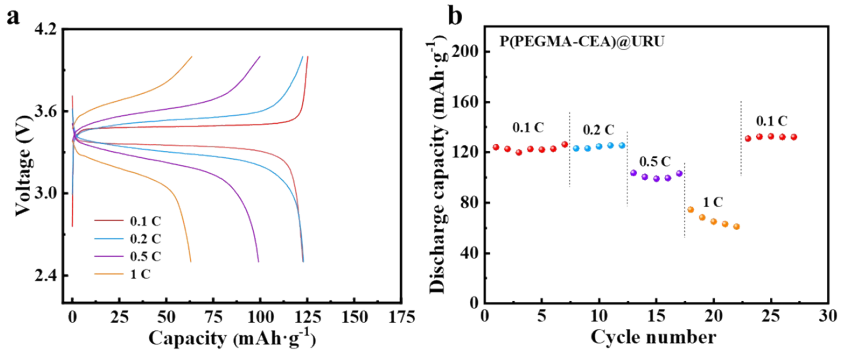

Fig. S24 (a) Typical charge/discharge curves of the Li|P(PEGMA-CEA)@URU|LFP battery. (b) Rate performance of the Li|P(PEGMA-CEA)@URU|LFP battery at 25 °C.

Table S6 Ionic conductivity, lithium-ion transference number, battery performance reported in the literature to date.

	Ionic conductivity	t_{Li+}	**Discharge Capacity**	**Refs.**
PEGMA /CEA/UPU	6.21×10^{-5} S·cm^{-1} (25 °C) 6.61×10^{-4} S·cm^{-1} (60 °C) 9.50×10^{-4} S·cm^{-1} (80 °C)	0.63 (25 °C)	25 °C - 0.2 C 159.7 mAh·g^{-1}	This work
PEGMA /MMA	2.81×10^{-6} S cm^{-1} (30 °C) 3.02×10^{-6} S cm^{-1} (30 °C)	0.37 (30 °C)	30 °C - 0.2 C 166.5 mAh·g^{-1}	6
PEO /DMMP	1.29×10^{-5} S cm^{-1} (25 °C)	0.46 (25 °C)	45 °C - 1 C 134.1 mAh·g^{-1}	7
PEO/OV-LLZTO	3.30×10^{-5} S cm^{-1} (30 °C) 5.60×10^{-4} S cm^{-1} (60 °C)	/	/	8
PEGME/BE	5.00×10^{-5} S cm^{-1} (90 °C)	0.92	/	9
PEO/ZIF-67 /CF/SN	1.17×10^{-4} S cm^{-1} (30 °C)	0.40 (30 °C)	25 °C - 0.2 C 152.5 mAh·g^{-1}	10
PEGMA /BtCOFs /LiTFSI	5.30×10^{-5} S cm^{-1} (25 °C)	0.47 (25 °C)	60 °C - 0.1 C 146.2 mAh·g^{-1}	11
PEO /LiTFSI /PI	6.80×10^{-5} S cm^{-1} (30 °C)	0.265	60 °C - 0.2 C 145.6 mAh·g^{-1}	12
PEO /LiBMB	0.45×10^{-3} S cm^{-1} (30 °C)	0.54 (30 °C)	60 °C - 0.1 C 145.5 mAh·g^{-1}	13

References

1. F. Neese, *WIREs Computational Molecular Science*, 2022, **12**, e1606.
2. F. Weigend, *Physical Chemistry Chemical Physics*, 2006, **8**, 1057-1065.
3. F. Weigend and R. Ahlrichs, *Physical Chemistry Chemical Physics*, 2005, **7**, 3297-3305.
4. M. A. Lee, J. B. Lee, J.-N. Lee, S.-G. Woo, J. Yu and H.-s. Kim, *Journal of Electroanalytical Chemistry*, 2022, **905**, 115900.
5. M. D. Hanwell, D. E. Curtis, D. C. Lonie, T. Vandermeersch, E. Zurek and G. R. Hutchison, *Journal of Cheminformatics*, 2012, **4**, 17.
6. L. Yu, Y. Zhang, J. Wang, H. Gan, S. Li, X. Xie and Z. Xue, *Macromolecules*, 2021, **54**, 874-887.
7. H. J. Cheon, T. T. Vu, M. Woo, Y. Kim, H. Choi, J. Kim, Y. Choi, Y. A. Kim, J. W. Yun, Y. Ko and M. Chang, *ACS Sustainable Chemistry & Engineering*, 2024, **12**, 2686-2699.
8. Y. Fu, K. Yang, S. Xue, W. Li, S. Chen, Y. Song, Z. Song, W. Zhao, Y. Zhao, F. Pan, L. Yang and X. Sun, *Advanced Functional Materials*, 2023, **33**, 2210845.
9. Y. Shao, F. Alloin, D. Bresser and c. Iojoiu, *Journal of Materials Chemistry A*, 2024, **12**, 30032-30040.
10. X. Song, K. Ma, J. Wang, H. Wang, H. Xie, Z. Zheng and J. Zhang, *ACS Nano*, 2024, **18**, 12311-12324.
11. X. Tan, Y. Tong, J. Yang, X. Du, A. Yang, A. Zhang and Q. Xu, *Polymer Chemistry*, 2024, **15**, 454-464.
12. Y. Li, Z. Fu, S. Lu, X. Sun, X. Zhang and L. Weng, *Chemical Engineering Journal*, 2022, **440**, 135816.
13. F. Yuan, L. Yang, X. Zou, S. Dong, S. Chi, J. Xie, H. Xing, L. Bian, L. Bao and J. Wang, *Journal of Power Sources*, 2019, **444**, 227305.